Available online at www.sciencedirect.com
ScienceDirect
Vibrational Spectroscopy 45 (2007) 71–81
VIBRATIONAL SPECTROSCOPY
www.elsevier.com/locate/vibspec

Review

The big picture of Raman scattering in carbon nanotubes

M.S. Dresselhaus [a,b], G. Dresselhaus [c,*], M. Hofmann [b]

[a] Department of Physics, Massachusetts nstitute of Technology, Cambridge, MA 02139-4307, United States
[b] Department of Electrical Engineering and Computer Science, Massachusetts Institute of Technology, Cambridge, MA 02139-4307, United States
[c] Francis Bitter Magnet Laboratory, Massachusetts Institute of Technology, Cambridge, MA 02139-4307, United States

Received 11 May 2007; received in revised form 6 July 2007; accepted 6 July 2007
Available online 24 July 2007

Abstract

A big picture view of Raman scattering in carbon nanotubes is presented, starting from its early history and the discovery of the unique Raman spectra of carbon nanotubes, and following on to the discovery of Raman spectra at the single nanotube level and a more detailed understanding of the scattering mechanism in terms of the excitonic picture. Recent developments and an outlook to the future of the field are emphasized along with the special role that Brazilian researchers have played in the development of the field. Both the advance in our understanding of Raman scattering in 1D systems and the use of Raman scattering to advance carbon nanotube research and sample characterization are discussed.

PACS : 78.67.Ch; 78.67. −n; 71.35.Cc

Keywords: Raman; Nanotubes

Contents

1. Introduction and early history . . . 71
2. Single SWNT Raman spectroscopy . . . 73
3. Excitonic interpretation of Raman spectra . . . 75
4. Current Raman studies and future outlook . . . 77
5. Outlook . . . 80
Acknowledgements . . . 80
References . . . 80

1. Introduction and early history

In this review of the big picture of Raman Scattering in carbon nanotubes, we emphasize both the evolution of this field over its 10-year history and the important role that Brazilian science has played in its evolution. Emphasis is given both to the impact that nanotubes have had on the evolution of Raman spectroscopy in one-dimensional systems and the impact that Raman spectroscopy has had on the development of carbon nanotube science and sample characterization.

Single walled carbon nanotubes (SWNTs) are unique in terms of their very small size (~ 1 nm in diameter), their strong one-dimensionality (1D), and the fact that a nanotube can be either semiconducting or metallic depending on the geometry which results from the rolling of the graphene sheet to form a SWNT as indicated in Fig. 1(a). Here we see the unusual electronic structure of graphene which has a dispersion relation linear in wave vector k about the K point in the Brillouin zone (Fig. 1(b)). The resulting conical constant energy surfaces of the valence and conduction bands touch at the K point of the Brillouin zone through which the Fermi energy passes (Fig. 1(b)). Thus two-dimensional graphene is by symmetry a zero-gap semiconductor. Since strong quantum confinement occurs in the two directions perpendicular to the nanotube axis,

* Corresponding author.
E-mail address: Millie@mgm.mit.edu (M.S. Dresselhaus).

0924-2031/$ – see front matter © 2007 Published by Elsevier B.V.
doi:10.1016/j.vibspec.2007.07.004

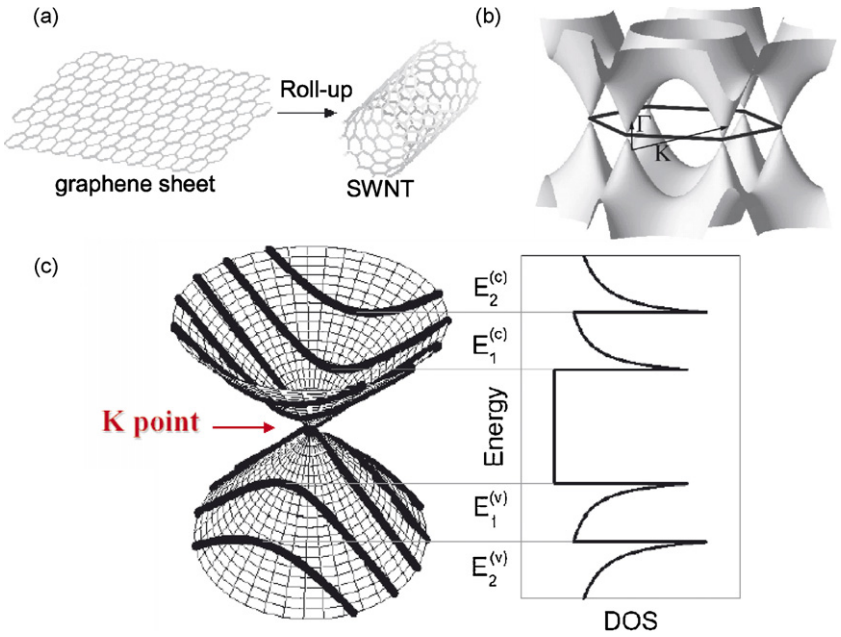

Fig. 1. (a) Rolling of a graphene sheet to form a SWNT. (b) Constant energy surfaces of 2D graphene showing a linear k dependence around the K point in the Brillouin zone. (c) The cutting lines (dark curves) intersecting the conical surfaces define the locus of allowed states for SWNTs and relate to the 1D electronic density of states (DOS) shown.

a quasi-continuum of states can only occur along the nanotube axis, resulting in the cutting lines shown in Fig. 1(c). These cutting lines are separated from one another by $2/d_t$, where d_t is the nanotube diameter, and the orientation of the cutting lines depends on the chiral angle θ of each nanotube, where θ is the angle between the chiral vector $C_h = n\hat{a}_1 + m\hat{a}_2$ and the $\hat{a}_1$ basis vector of graphene. Thus every (n,m) nanotube has a unique set of cutting lines resulting in a unique set of energy levels $E_n(k)$. If one of the cutting lines goes through the K point (Fig. 1(c)), then the SWNT is metallic with occupied states at the K point. The characteristic van Hove singularities (vHSs) associated with 1D systems are seen at the extremal point of each cutting line (Fig. 1(c)). If the SWNT is undoped, the Fermi level of the SWNT will then lie halfway between the highest lying vHS in the valence band and the lowest lying one in the conduction band. Furthermore, each (n,m) SWNT will have a unique set of vHSs, corresponding to energies E_i with a very high density of electronic states (Fig. 1(c)). This density of states can be probed experimentally, and in fact by the Raman effect. However the optical transitions for nanotubes are excitonic and are strongly influenced by many body interactions, as discussed below.

The first experimental study of the Raman effect in SWNTs started 10 years ago, when for the first time a sufficient supply of SWNTs became available through a breakthrough in the synthesis process that occurred in Smalley's group at Rice University [1]. The Raman spectra thus obtained (see Fig. 2(b)) showed the two characteristic and unique signatures of carbon nanotubes [2]. The first signature relates to the G-band arising from the optical vibration of two adjacent carbon atoms on the wall of the SWNT, which for semiconducting tubes shows a doublet structure with a strong G^+peak, associated with vibrations along the tube and identified with the LO (longitudinal optical) mode, and a weaker G^- peak appearing at a little lower frequency, associated with vibrations in the circumferential direction and identified with the TO (transverse optical) mode, and softened by the curvature of the nanotube. The down-shift of ω_{G^-} relative to ω_{G^+} is due to an admixture of a small amount of a low frequency phonon mode normal to the graphene sheet. For metallic tubes the G^+ mode is associated with the TO mode and the LO mode lies at a lower frequency because of the strong electron phonon interaction and the Kohn anomaly [3–5]. The second characteristic signature of a SWNT is the appearance of a strong Raman feature at relatively low frequencies, associated with the radial breathing mode (RBM) where all the carbon atoms are vibrating in the radial direction in an A-symmetry totally symmetric breathing mode pattern, unique to SWNTs. The vibrational frequency ω_{RBM} was identified with a $1/d_t$ diameter dependence [2], thus providing a method for characterizing the diameter distribution in the SWNT ensemble samples available at that time. The strong dependence of the two characteristic Raman features on laser excitation energy E_{laser} was interpreted in terms of a resonance Raman scattering (RRS) process discovered earlier by two Brazilian scientists (Leite and Porto) when they were working at Bell Labs in the US in their early careers [6]. According to the RRS process, a strong Raman intensity is only observed for those (n,m) tubes with singularities in their joint density of states in resonance with E_{laser}. According to this RRS process, the laser energy E_{laser} selects only those (n,m) SWNTs with optical transition energies within the resonance window of E_{laser}, as illustrated in Fig. 2(a). From the relation between the radial breathing mode frequency ω_{RBM} and the tube diameter d_t, it became clear that the Raman effect could provide important information on the characterization of the (n,m) nanotube distribution contained within typical ensemble samples.

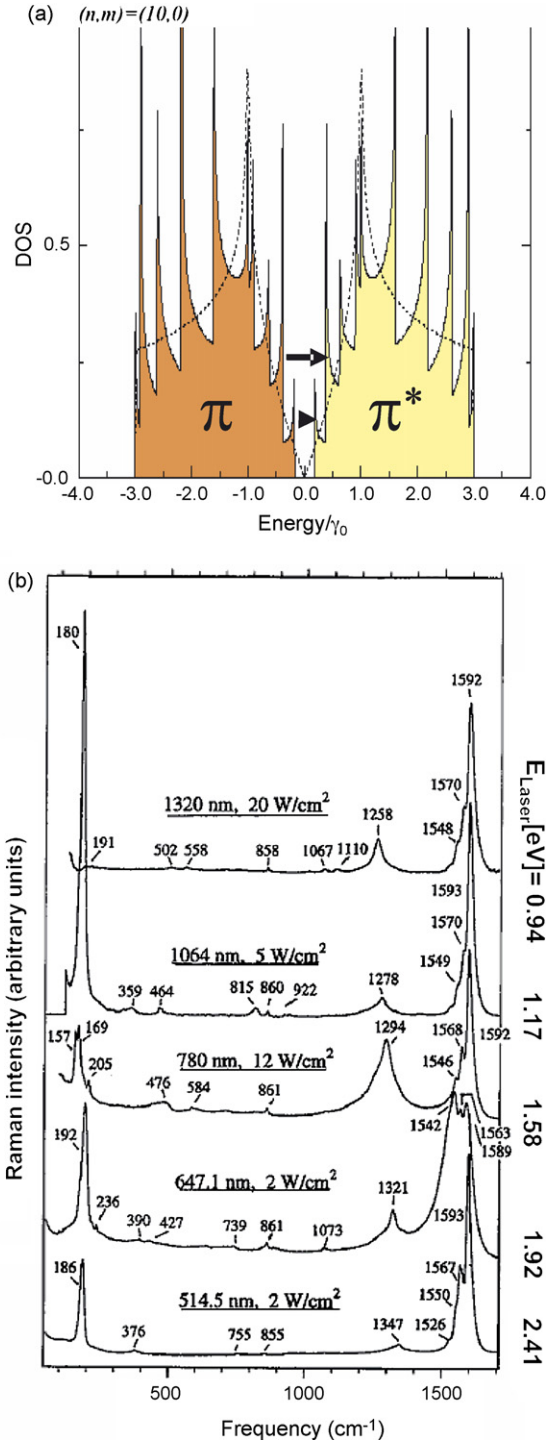

Fig. 2. (a) The density of electronic states (DOS) in the valence and conduction bands. The arrows show the energy separation between two singularities in the DOS in the conduction and valence bands coupled by light. (b) Raman spectra for the same SWNT sample taken at different values of E_{laser} [2].

The next breakthrough that occurred in the history of the Raman effect in carbon nanotubes came in 1998, through another Brazilian, Marcos Pimenta, who when visiting MIT did a systematic study of the Raman spectra in SWNT ensemble samples, following up on the early work of Rao et al. [2] but now using many more laser lines [7,8]. In his studies he noticed that for the diameter distribution of his sample, the spectral lineshape was dependent on E_{laser} (see Fig. 3(a)), showing one type of lineshape which he identified with semiconducting S-SWNTs, but for E_{laser} in the range between 1.83 and 2.14 eV, a very different lineshape was identified and associated with metallic M-SWNTs. From the Kataura plot shown in Fig. 3(b), where the resonant energies of all the E_{ii} transition for every (n, m) nanotube are plotted in accordance with the RRS process indicated by Fig. 2(a) and a simple tight binding model for the electronic structure of SWNTs, it became clear that when E_{laser} was in resonance primarily with M-SWNTs, a different lineshape was observed than for S-SWNTs. This finding came at about the same time as it was shown experimentally using low temperature scanning probe spectroscopy and scanning tunneling microscopy [9,10] that SWNTs could be either S-SWNTs or M-SWNTs depending on their nanotube (n, m) chirality, as had been predicted previously [11,12]. Showing that similar information could be obtained with Raman spectroscopy, a technique generally available to most experimental groups, was a significant breakthrough at that time for making possible a much more detailed characterization of the (n, m) SWNTs contained within the SWNT ensemble (or rope) samples that were available at that time.

2. Single SWNT Raman spectroscopy

The second phase of advances in Raman spectroscopy relates to the observation of spectra at the single nanotube level [13], as shown in Fig. 4. Here, examples of Raman spectra for one individual metallic (upper trace) and one semiconducting (lower trace) SWNT are shown, as observed by another Brazilian [13], Ado Jorio, working in his early career at MIT. The observation of spectra at the single nanotube level is enabled by the strong enhancement in intensity occurring because of the 1D nature of the electronic density of states, so that the intensity of the RBM feature (see insets to Fig. 5 for the carbon atom mode displacements) from one SWNT is comparable to the signal coming from the many silicon atoms illuminated by the 1 μm light beam on the substrate (Fig. 4). From measurement of the RBM frequency and the resonant energy of each (n, m) tube, the Kataura plot (see Fig. 3(b)) allowed identification of the (n, m) identity of individual tubes. The determination of the resonant energy within the resonance window over which a given (n, m) tube could be observed was enabled by analysis of the Stokes and anti-Stokes features of the Raman spectra carried out by another Brazilian doctoral student, Antonio G. Souza-Filho [14,15].

Having shown that Raman spectra at the single nanotube level could be observed, the properties of each of the features normally observed in the Raman spectra of SWNTs (see Fig. 5) could be explored as a function of diameter and chiral angle. Both first-order Raman features, such as the RBM and the *G*-band, and second order features, such as the *D*-band and G'-band (in Fig. 5), could be studied in this way. As an example of first-order G-band spectra, we show the spectra for three semiconducting tubes (Fig. 6(a)) and for three metallic tubes (Fig. 6(b)) [16], yielding the diameter

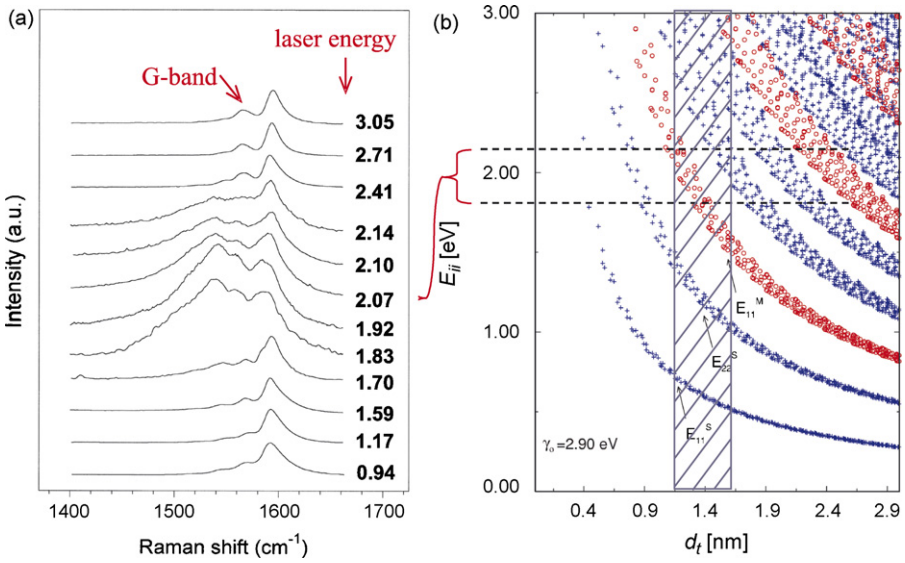

Fig. 3. (a) G-band spectra for SWNT ensemble samples with a diameter range indicated by the cross hatched strip in (b) where a Kataura plot of resonant energies for optical transitions are plotted vs. SWNT diameter d_t based on a simple tight binding calculation of the electronic structure. Note the difference in the lineshape of the G^- feature for S-SWNTs and M-SWNTs [8].

dependence of the G^- feature shown in Fig. 6(c). The G^+ feature was seen to have little diameter dependence. Line shapes at the individual tube level for S-SWNTs similar to that of ensemble samples (Fig. 3) could be seen, while that for M tubes showed a variety of lineshapes. Interestingly, the lineshape of M-SWNTs at the single nanotube level remained an open issue for some time. It was not until several years later with the identification of the Kohn anomaly [3–5] that this topic is being clarified. For the S-SWNTs, polarization studies at the single nanotube level [17] identified the detailed lineshape and the symmetries of the six symmetry components contributing to the complex lineshape identified in the initial observation of Raman spectra for SWNTs [2]. Polarization studies of M-SWNTs are more complicated because of the dependence of the lineshapes of the spectra on chirality and laser energy dependence, and though they have been carried out over a period of time, such polarization studies still remain an area of active study. Furthermore, studies at the single nanotube level clarified understanding of the Raman spectra of bundled samples where contributions are observed from both metallic and semiconducting tubes and where perturbations due to inter-tube interactions are also observed.

The behavior of the second order D-band and G'-band features were also clarified by studies at the single nanotube level which illuminated the physical characteristics of these highly dispersive features through the double resonance process which enables the G'-band to have such a strong intensity [18–22]. The large dispersion of the G'-band frequency with E_{Laser} enabled study of the wave vector dependence of Raman features, allowing analysis to be made of the trigonal

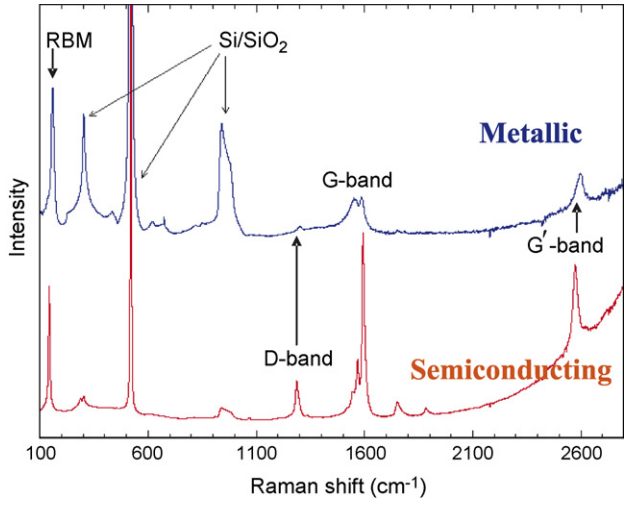

Fig. 4. Raman spectrum for an individual metallic SWNT (upper trace) and a semiconducting SWNT (lower trace) showing a signal comparable to the Raman intensity from the substrate Si atoms. Adapted from Ref. [13].

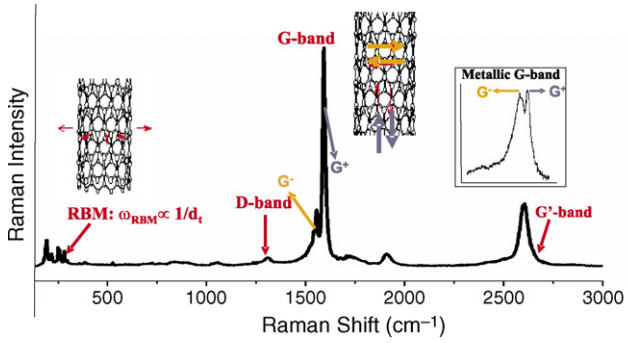

Fig. 5. Raman spectra from a bundle SWNT sample containing both S-SWNTs and M-SWNTs, showing the radial breathing mode (RBM, left inset), the G-band for S-SWNTs in resonance (center inset), and the G-band lineshape for M-SWNTs in resonance with E_{laser} (right inset). Also featured is the G'-band which is the second order peak of the D-band, but by symmetry, the G'-band is Raman-allowed and is not defect-induced.

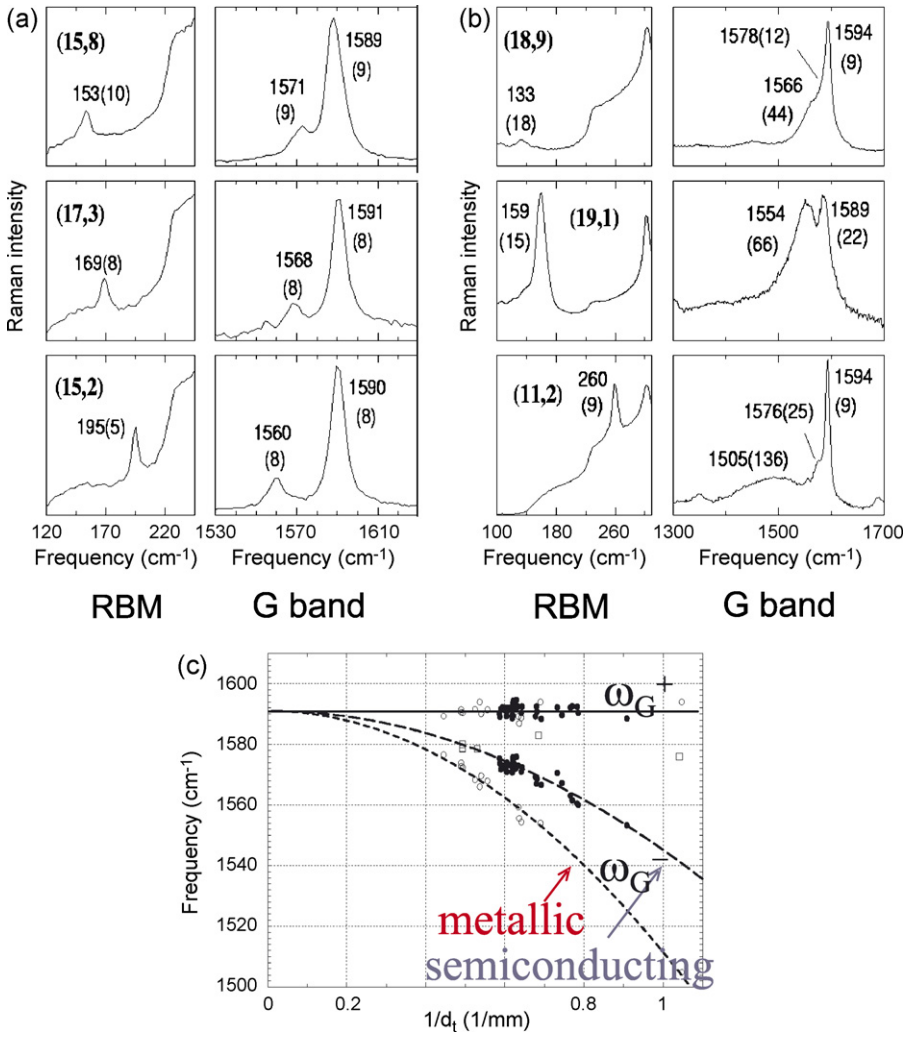

Fig. 6. The RBM and G-band spectra for three S-SWNTs (a) and three M-SWNTs (b) with frequencies (linewidths) given. (c) The G^+-band shows almost no dependence on the diameter or chiral angle, while the G^--band shows a downshift that depends strongly on tube diameter (as $1/d_t^2$). Adapted from Ref. [16].

warping effect on the electronic structure of SWNTs [23](see Fig. 7) and later of the trigonal warping effect of the phonon modes, once further understanding was obtained of the connection between cutting lines and the double resonance process [24,25]. Since the D-band and G'-band arise from highly dispersive double resonance processes, the D-band and G'-band frequencies depend both on the tube diameter and on the laser excitation energy which can be studied at the single nanotube level [26].

Another major impact of single nanotube spectroscopy is on the metrology of nanotubes, allowing a detailed examination of the physical properties of individual nanotubes to be made by performing joint Raman experiments to identify the chiral indices of a particular (n, m) SWNT and then to measure its physical properties, such as its transport I–V characteristics or its strain behavior [28–30]. The observation of the Raman effect at the single nanotube level inspired exploration of other photo-physical effects that could also be observed at the single nanotube level, and launched the third phase of Raman spectroscopy studies in SWNTs which is discussed next.

3. Excitonic interpretation of Raman spectra

The observation of the fluorescent emission of light by SWNTs (wrapped in a surfactant sodium dodecyl sulfate (SDS)) at energy E_{11} after excitation at E_{22} (see Fig. 8(b)) ushered in the third phase of the history of Raman spectroscopy in carbon nanotubes. Characteristic of this phase of Raman spectroscopy in SWNTs was the introduction of other complementary spectroscopies that could be performed at the single nanotube level and the discovery that optical transitions in SWNTs are excitonic, and strongly dependent on many-body effects [31]. Photoluminescence spectroscopy (PL) has provided a complementary tool for the (n, m) chirality identification of semiconducting SWNTs [32,33], as shown in Fig. 8. Here, only those isolated SWNTs that are wrapped in a surfactant such as SDS can be in excited states long enough to emit light before recombination occurs. In the early PL studies, absorption occurred at E_{22}^S and emission at E_{11}^S (Fig. 8(b)).

The photoluminescence emission from SWNTs in solution is shown in Fig. 8(c) as a function of absorption excitation wave

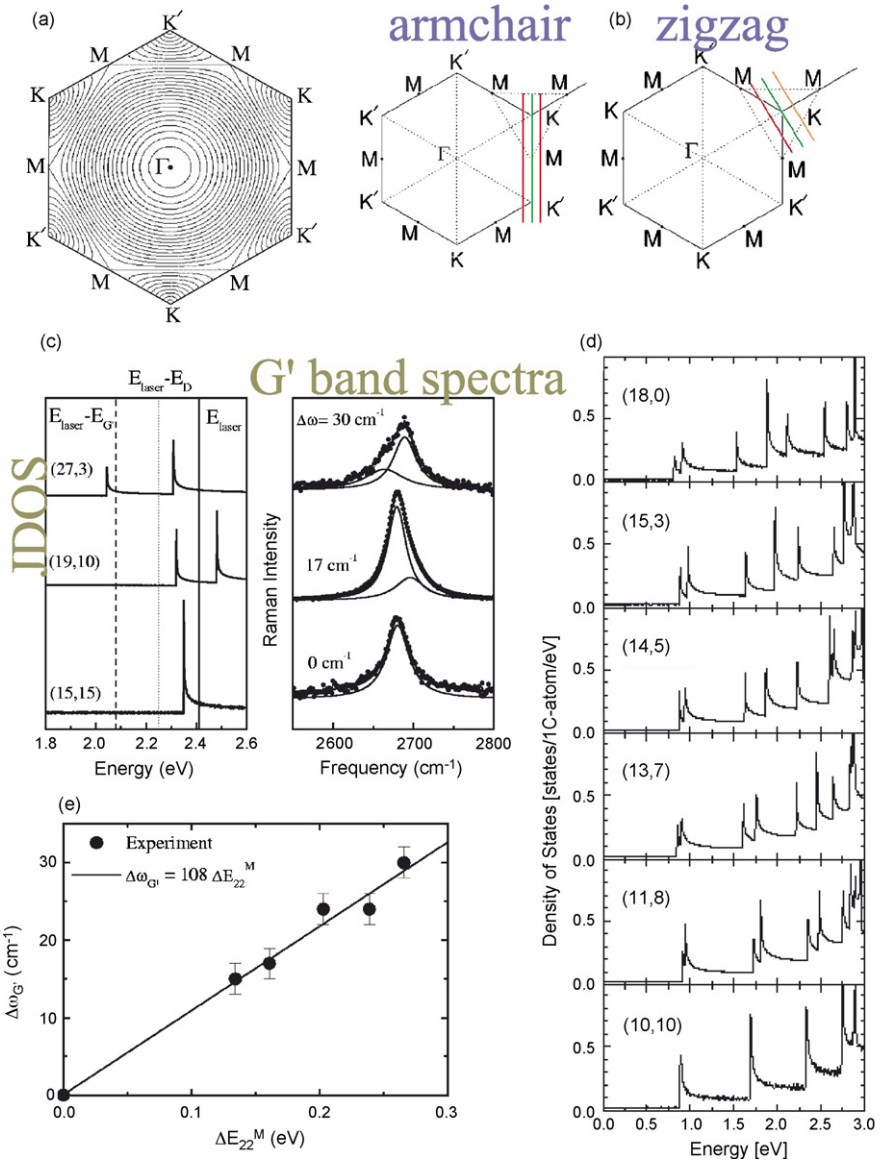

Fig. 7. (a) Constant energy contours showing the trigonal warping effect for k vectors moving away from the K point. (b) The symmetric arrangement of the cutting lines for armchair tubes in contrast to the non-symmetric arrangement for zigzag tubes, giving rise to a splitting of each vHS, which is shown in (d) to increase as the chiral angle in decreased from 30° for armchair tubes to 0° for zigzag tubes. (c) Examples of G'-band spectra showing splittings associated with trigonal warping effects. (e) Relation between splitting of the G'-band Raman frequency and of the splitting of the E_{22}^{M} van Hove singularity (vHS). Adapted from Refs. [23,27].

lengths (which can also be expressed on an energy scale). When the energies for these optical excitations are then plotted on a Kataura plot, it is seen that the experimental points are arranged according to family patterns mod$((2n + m), 3)$ and the E_{22}^{S}/E_{11}^{S} transition energy ratios are not 2, as would be expected for an electronic structure calculation based on the simple tight binding model, but this ratio was rather found to be 1.8 (called the ratio problem).

Furthermore, the actual identification of the chiral indices (n, m) by the RRS method and by the PL method did not seem to be consistence with one another. To gain further insight into this problem, RRS and PL measurements were made on the same SDS-wrapped SWNT sample [34]. Then the same E_{ii} values were obtained for the same (n, m) tubes, thereby resolving this issue about the observation of family effects in SWNTs. The ratio problem on the other hand, presented unexplained fundamental physics phenomena, whose resolution ultimately led to the interpretation of the optical excitation process in SWNTs in terms of excitonic processes [31]. From another standpoint, the observation of three-dimensional PL emission intensity maps versus E_{22}^{S} absorption/ E_{11}^{S} emission energy as in Fig. 8, stimulated the development of experimental Raman methods for using many laser excitation line mapping, as shown in Fig. 9. This advance enriched the development of RRS techniques for nano-systems in studies of the Raman lineshape within the resonant window of SWNTs. These mapping techniques also became common for the spatial mapping of the intensities of specific Raman features, such as the RBM and the G-band, thereby facilitating the study of environmental effects, such as might be introduced by SWNTs sitting on substrates, through

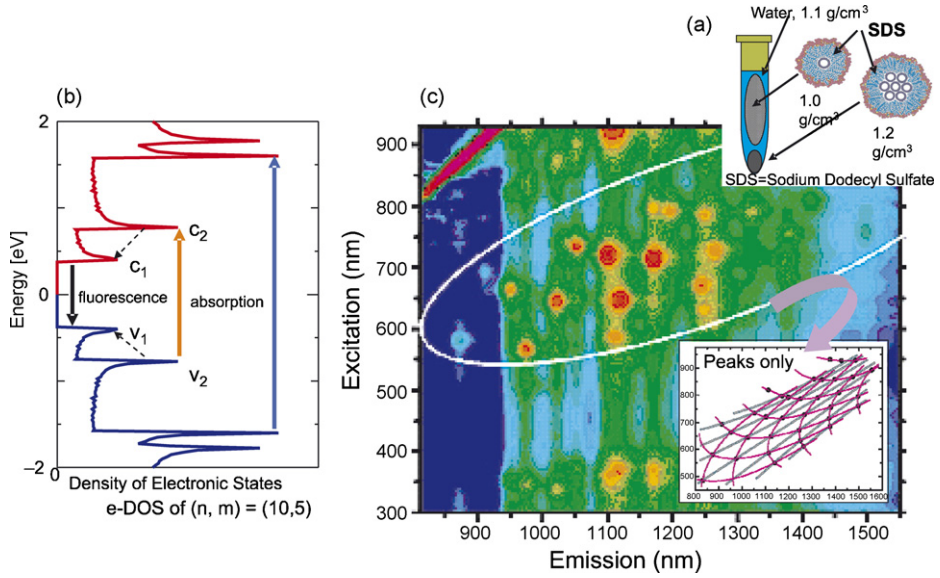

Fig. 8. Photoluminescence in carbon nanotubes: (a) Observation is enabled by the wrapping of individual SWNTs with a surfactant and the separation of these species for access by an optical beam. (b) model of PL process as absorption of light at E_{22}^{S} and emission at E_{11}^{S}. (c) Plot of resonance excitation vs. resonant PL emission. The inset shows family patterns. Adapted from Refs. [32,33].

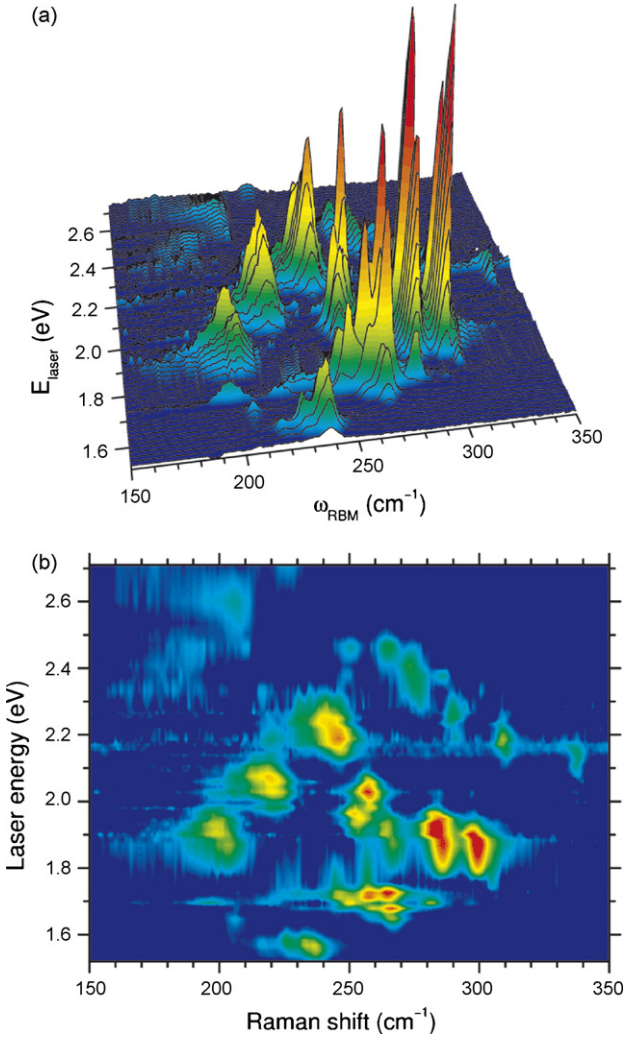

Fig. 9. (a) 3D map of the intensity of the resonance Raman energies vs. ω_{RBM} and (b) the corresponding 2D projection of this map on the E_{ii} vs. ω_{RBM} plane [34].

comparative lineshape studies such as that for freely suspended nanotubes and those sitting on substrates (Fig. 10).

From a more fundamental standpoint the joint RRS and Raman studies led to the development of the extended tight binding model, which included consideration of SWNT curvature effects, long-range C–C bonding interactions, and geometrical structure optimization [36,37]. With the extended tight binding model, the photo-physical properties of SWNTs could be more effectively explored in studying phenomena such as strain effects in carbon nanotubes [30], studying double walled carbon nanotube (DWNT) spectroscopy [38], the role of linear carbon chains in DWNT coalescence [39], and a comparative study of bromine intercalation of graphite and of DWNT bundles [38].

4. Current Raman studies and future outlook

As we look into the start of the second decade of the use of Raman spectroscopy to study carbon nanotubes, we see the same two trends of the first decade still remaining in sharp focus, but also with some new emphasis. The two continuing themes include new fundamental studies in the Raman spectroscopy of 1D systems as well as advances in the characterization of carbon nanotubes, which we illustrate below with several examples.

To study the comparative intercalation of graphite and DWNT bundles, bromine was at first selected for the intercalant, because it allowed investigation of the effect of intercalation on both the bromine guest and the DWNT host species. The inset to Fig. 11 shows the structural effect of bromine doping on DWNTs, indicating that intercalation preserves the structural integrity of the DWNTs, and suggesting that the bromine intercalant enters between the outer walls of the DWNTs [38] in much the same way that it goes between adjacent graphene layers in graphite intercalation compounds

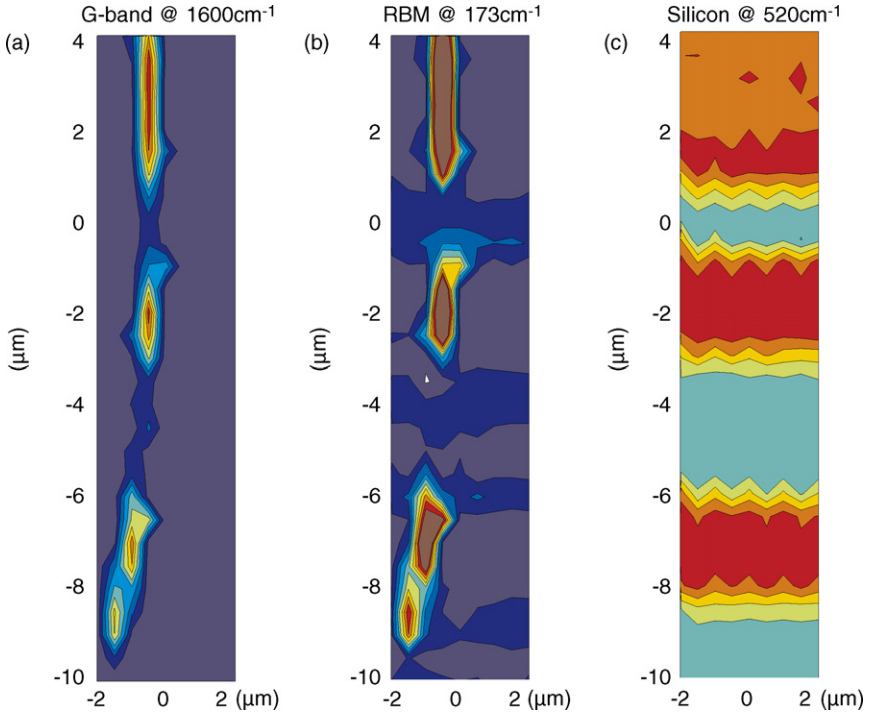

Fig. 10. Spatial maps of resonant Raman scans along the length of an individual nanotube for (a) the *G*-band, (b) the RBM feature and (c) Raman scans in the light area corresponding to the location of Si posts across which the SWNT in (a) and (b) was suspended [35].

[40]. The effect of intercalation on the bromine breathing mode can be seen in Fig. 11 where a new feature is seen in the Raman spectra taken at $E_{laser} = 2.33$ eV of bromine-intercalated DWNTs where a strong feature is seen at 233 cm^{-1} in intercalated DWNTs, but is not seen in unintercalated DWNTs. The observed frequency for the Br–Br stretch mode is consistent with theoretical density functional calculations within the local density approximation [41]. This Br–Br vibrational mode is resonant in the spectra near 2.33 eV, and the bromine diatomic breathing mode peak is downshifted by 91 cm^{-1} relative to its counterpart in the gas phase. On the other hand, the RBM of the outer semiconducting tube does not shift in frequency with bromine intercalation but the RBM of the inner metallic tube downshifts in frequency and decreases in intensity with 2.33 eV excitation, as can be seen in Fig. 12 showing bromine intercalated DWNT bundle subjected to a heating and cooling cycle. Unlike the situation in graphite intercalation compounds (GICs) where it is difficult to completely drive out the bromine [40], heating of the Br_2-DWNT sample to 150° C is

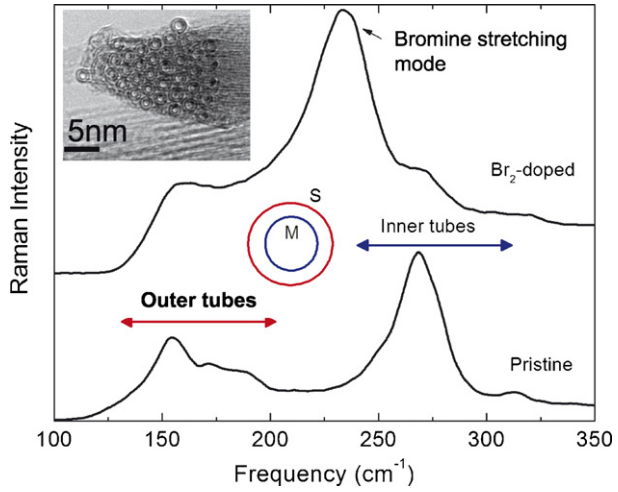

Fig. 11. Raman spectra taken at 2.33 eV for a sample of DWNTs before and after Br_2 doping where E_{laser} is in resonance with the outer semiconducting tubes and inner metallic tubes for the pristine sample, but for the bromine-doped sample the bromine stretching mode dominates the spectrum. The inset on the upper left shows that the bromine doping does not destroy the crystalline arrangement of the DWNTs [38].

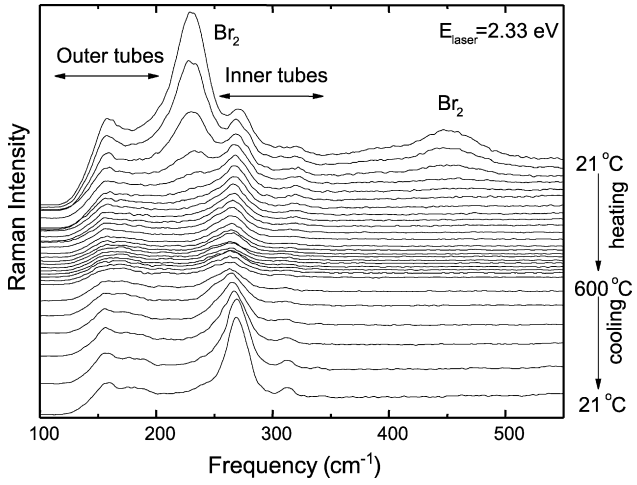

Fig. 12. Raman spectra taken on a sample of Br_2-adsorbed DWNTs at different temperatures (increments in *T* are 25° C on the heating cycle to 600° C and are 100° C on the cooling cycle). Adapted from Ref. [38]. Initially at 21° C a strong signal is seen at 233 cm^{-1} from the Br_2-intercalated sample and at its second harmonic [38].

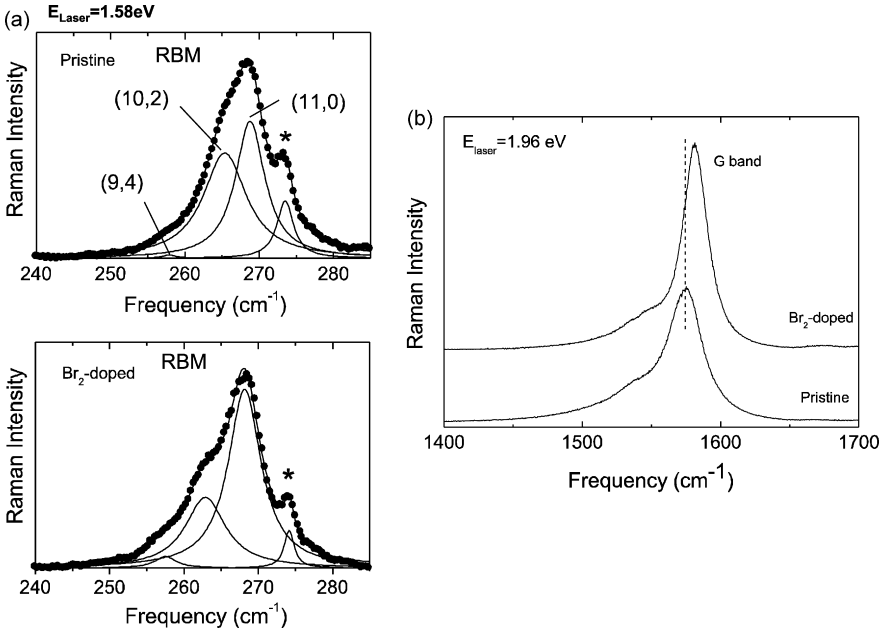

Fig. 13. (a) For $E_{laser} = 1.58$ eV, the RBM features for individual tubes can be identified and monitored as the Br_2dopant is added. (b) For 1.96 eV, a 7 cm^{-1}up-shift in the G^+ peak is found upon bromine addition (acceptor doping [38]).

sufficient to drive out the bromine from the intercalation compound and to restore the initial Raman spectrum before bromine addition (see Fig. 12). Also unlike the situation in GICs, when the inner tube is metallic, then intercalation with bromine up-shifts the G^+-band (by 7 cm^{-1}in the case of Fig. 13(b) where 1.98 eV excitation is used), whereas when the inner tube is semiconducting (excitation of 1.58 eV) no shift of the G^+-band is observed, suggesting that charge transfer effects occur between inner and outer tubes of DWNTs for the S/M configuration for the outer/inner tubes. Consistent results were also obtained by Barros, a Brazilian graduate student working on the H_2SO_4–DWNT system [42].

The use of Raman spectroscopy for the characterization and metrology of SWNTs has also been advanced recently. An example of this research direction of the field is the final topic of this big picture overview which relates to a study of the *D*-band in the Raman spectra of SWNTs. This feature has been used from the beginning of time [2] to evaluate the amount of disorder in a SWNT sample. A major advance in this characterization of carbon nanotubes occurred with recent findings by a Brazilian group [43], that the laser energy dependence of the *D*-band in graphite could be expressed in terms of a universal relation $L_a(\text{nm}) = (560/E^4_{laser})(I_D/I_G)^{-1}$.

An extension of these ideas was subsequently made by studying the dependence of the normalized *D*-band intensity of SWNTs on nanotube length [44]. In this work it was shown that when the tube length L_{tube} becomes less than about 100 nm (corresponding to less than half the wavelength λ of the laser excitation), then the ratio I_D/I_G starts to show an increase with decreasing L_{tube}, obeying a dependence of $I_D/I_G \sim 1/L_{tube}$, as if L_{tube} played the role of a mean free path of SWNT carriers, a role similar to that played by the in-plane structural coherence distance L_a in graphite. In this work [44] the SWNT length dependence of I_D/I_G was measured on four samples. The first was a control sample (called as-grown) showing the same diameter distribution as the other three samples, but having a normal length distribution (greater than $\lambda/2$), while the three short samples had lengths L_{tube} of 100 nm, 70 nm and 50 nm. Fig. 14 shows that the *D*-band intensity at 647 nm laser excitation ($E_{laser} = 1.917$ eV) for the three short samples increased as L_{tube} decreased, and Fig. 15 showed that I_D/I_G follows a $1/L_{tube}$ dependence for four different laser excitation energies. From these results we conclude that: (1) L_{tube} plays the role of a symmetry-breaking perturbation (similar to L_a) for sufficiently short tubes), (2) normal scattering processes are dominant for tubes longer or equal to 100 nm, (3) L_{tube} plays a role similar to L_a in inducing disorder in the Raman scattering process for short

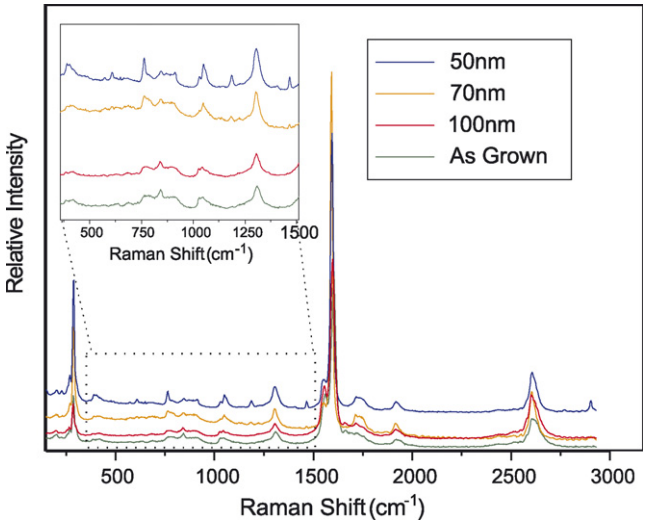

Fig. 14. Raman spectra are shown for four samples with tubes of different lengths. A zoom of the spectrum between 500 and 1500 cm^{-1} highlights the increase in the *D*-band intensity as the tube length decreases [44].

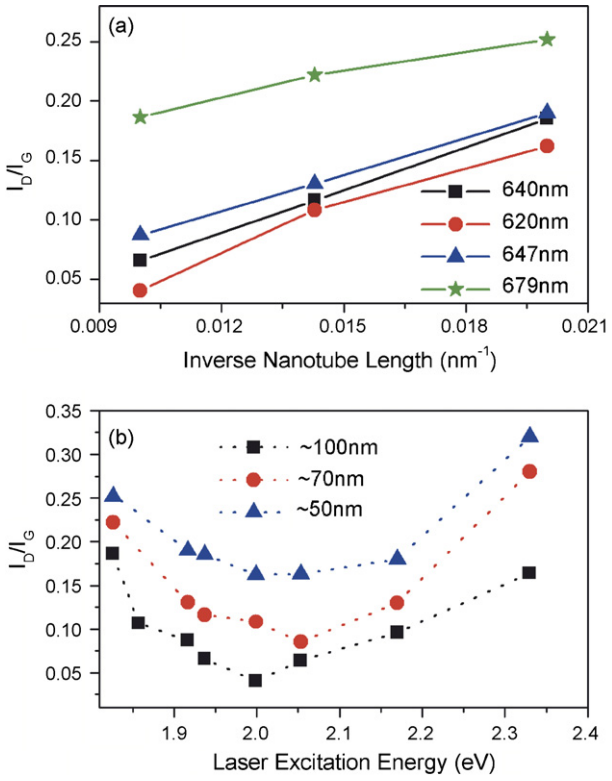

Fig. 15. (a) Plot of I_D/I_G vs. $1/L_{tube}$ for different laser excitation wavelengths (energies) showing larger I_D/I_G for M-SWNTs in comparison to S-SWNTs. (b) Plot of the I_D/I_G ratio vs. E_{laser} showing a similar result as in (a) [44].

tubes, (4) M tubes (in resonance with $E_{laser} = 2.3$ eV) showed a much larger I_D/I_G ratio than S tubes (in resonance with the other E_{laser} excitation energies). Curiously M-SWNTs show a dependence of I_D/I_G on E_{laser} consistent with that of graphite, meriting further study, (5) S-SWNTs consistently show a weaker *D*-band feature, for the same L_{tube} distribution and sample preparation method, also meriting further investigation.

5. Outlook

This study on short SWNTs is part of recent interest in developing a metrology science for nanotubes, whereby RRS would become one of the major characterization techniques to be used for the specification of SWNT samples that would eventually be used in the market place for supplying SWNTs commercially and in large scale for specific applications. This developing interest in metrology is part of a growing trend of increasing numbers of new entrants to the nanotube R&D field coming from the applications sector. Interest in nanotube metrology also comes from researchers focused on SWNT synthesis scale-up strategies. To address these trends, the Brazilian nanotube metrology efforts are now assuming a leadership position by sponsoring a satellite conference on nanotube metrology in Rio de Janeiro in June 2007 in connection with the upcoming international congress to be held in Ouro Preto, Brazil in June 2007.

In looking toward the large role that Brazilian science has been playing in the area of Raman spectroscopy of carbon nanotubes over the history of the subject, it seemed appropriate to open the international workshop on Raman spectroscopy in Fortaleza, Brazil (September, 2006) with a big picture overview of Raman spectroscopy for the past decade with a view toward new developments expected in the next decade both in fundamental scientific studies which are emphasized at the Fortaleza conference but also on practical aspects which are likely to become of increasing importance worldwide in the future if the nanotube field is going to achieve its full potential in the commercial sector in service to societal needs.

Acknowledgements

The MIT authors acknowledge support under NSF Grant DMR 04-05538.

References

[1] A. Thess, R. Lee, P. Nikolaev, H. Dai, P. Petit, J. Robert, C. Xu, Y.H. Lee, S.G. Kim, A.G. Rinzler, D.T. Colbert, G.E. Scuseria, D. Tománek, J.E. Fischer, R.E. Smalley, Science 273 (1996) 483–487.
[2] A.M. Rao, E. Richter, S. Bandow, B. Chase, P.C. Eklund, K.W. Williams, S. Fang, K.R. Subbaswamy, M. Menon, A. Thess, R.E. Smalley, G. Dresselhaus, M.S. Dresselhaus, Science 275 (1997) 187–191.
[3] M. Lazzeri, et al. Phys. Rev. B 73 (2006) 155426.
[4] V.N. Popov, P. Lambin, Phys. Rev. B 73 (2006) 085407.
[5] K.T. Nguyen, A. Gaur, M. Shim, Phys. Rev. Lett. 98 (2007) 145504.
[6] R.C.C. Leite, S.P.S. Porto, Phys. Rev. Lett. 17 (1966) 1012.
[7] M.A. Pimenta, A. Marucci, S.D.M. Brown, M.J. Matthews, A.M. Rao, P.C. Eklund, R.E. Smalley, G. Dresselhaus, M.S. Dresselhaus, J. Mater. Res. 13 (1998) 2396–2404.
[8] M.A. Pimenta, A. Marucci, S. Empedocles, M. Bawendi, E.B. Hanlon, A.M. Rao, P.C. Eklund, R.E. Smalley, G. Dresselhaus, M.S. Dresselhaus, Phys. Rev. B: Rapid 58 (1998) R16016–R16019.
[9] J.W.G. Wildoer, L.C. Venema, A.G. Rinzler, R.E. Smalley, C. Dekker, Nature 391 (1998) 59.
[10] T.W. Odom, J.-L. Huang, P. Kim, C.M. Lieber, Nature 391 (1998) 62.
[11] R. Saito, M. Fujita, G. Dresselhaus, M.S. Dresselhaus, Phys. Rev. B 46 (1992) 1804–1811.
[12] R. Saito, M. Fujita, G. Dresselhaus, M.S. Dresselhaus, Appl. Phys. Lett. 60 (1992) 2204–2206.
[13] A. Jorio, R. Saito, J.H. Hafner, C.M. Lieber, M. Hunter, T. McClure, G. Dresselhaus, M.S. Dresselhaus, Phys. Rev. Lett. 86 (2001) 1118–1121.
[14] A.G. Souza Filho, A. Jorio, J.H. Hafner, C.M. Lieber, R. Saito, M.A. Pimenta, G. Dresselhaus, M.S. Dresselhaus, Phys. Rev. B 63 (2001) 241404R.
[15] A.G. Souza Filho, Electronic, structural and vibrational properties of carbon nanotubes and ferroelectric system $PbZr_{1-x}Ti_xO_3$ (in Portuguese), PhD thesis, Universidade Federal do Ceará, Fortaleza-CE, 60455-760, Brazil, Departamento de Física, December 2001.
[16] A. Jorio, A.G. Souza Filho, G. Dresselhaus, M.S. Dresselhaus, A.K. Swan, M.S. Ünlü, B. Goldberg, M.A. Pimenta, J.H. Hafner, C.M. Lieber, R. Saito, Phys. Rev. B 65 (2002) 155412.
[17] A. Jorio, G. Dresselhaus, M.S. Dresselhaus, M. Souza, M.S.S. Dantas, M.A. Pimenta, A.M. Rao, R. Saito, C. Liu, H.M. Cheng, Phys. Rev. Lett. 85 (2000) 2617–2620.
[18] C. Thomsen, S. Reich, Phys. Rev. Lett. 85 (2000) 5214.
[19] R. Saito, A. Grüneis, Ge.G. Samsonidze, V.W. Brar, G. Dresselhaus, M.S. Dresselhaus, A. Jorio, L.G. Cançado, C. Fantini, M.A. Pimenta, A.G. Souza Filho, N. J. Phys. 5 (2003) 157.1–15715.15715.
[20] C. Thomsen, S. Reich, Phys. Stat. Sol. B 225 (2001) R18–R19.
[21] C. Thomsen, S. Reich, Philos. Trans. R. Soc. 362 (2004) 2271–2288.
[22] J. Maultzsch, R. Pomraenke, S. Reich, E. Chang, D. Prezzi, A. Ruini, E. Molinari, M.S. Strano, C. Thomsen, C. Lienau, Phys. Rev. B 72 (2005) 241402.

[23] A.G. Souza Filho, A. Jorio, Ge.G. Samsonidze, G. Dresselhaus, M.S. Dresselhaus, A.K. Swan, M.S. Ünlü, B.B. Goldberg, R. Saito, J.H. Hafner, C.M. Lieber, M.A. Pimenta, Chem. Phys. Lett. 354 (2002) 62–68.
[24] Ge.G. Samsonidze, R. Saito, A. Jorio, A.G. Souza Filho, A. Grüneis, M.A. Pimenta, G. Dresselhaus, M.S. Dresselhaus, Phys. Rev. Lett. 90 (2003) 027403.
[25] Ge.G. Samsonidze, R. Saito, A. Jorio, M.A. Pimenta, A.G. Souza Filho, A. Grüneis, G. Dresselhaus, M.S. Dresselhaus, J. Nanosci. Nanotechnol. 3 (2003) 431–458.
[26] A.G. Souza Filho, A. Jorio, Ge.G. Samsonidze, G. Dresselhaus, M.A. Pimenta, M.S. Dresselhaus, A.K. Swan, M.S. Ünlü, B.B. Goldberg, R. Saito, Phys. Rev. B 67 (1–7) (2003) 035427.
[27] M.S. Dresselhaus, G. Dresselhaus, R. Saito, A. Jorio, Phys. Rep. 409 (2005) 47–99.
[28] S.B. Cronin, R. Barnett, M. Tinkham, S.G. Chou, O. Rabin, M.S. Dresselhaus, A.K. Swan, M.S. Ünlü, B.B. Goldberg, Appl. Phys. Lett. 84 (2004) 2052–2055.
[29] A.G. Souza Filho, N. Kobayasi, J. Jiang, R. Saito, S.B. Cronin, J. Mendes Filho, Ge.G. Samsonidze, G. Dresselhaus, M.S. Dresselhaus, in: C.S. Ozkan, F. Rosei, G.P. Lopinski, Z.L. Wang (Eds.), Assembly at the Nanoscale—Toward Functional Nanostructured Materials (Mater. Res. Soc. Symp. Proc. 910E), Materials Research Society Press, Warrendale, PA, 2006, 0901-Rb24-04 pp.
[30] A.G. Souza Filho, N. Kobayasi, J. Jiang, A. Grüneis, R. Saito, S.B. Cronin, J. Mendes Filho, Ge.G. Samsonidze, G. Dresselhaus, M.S. Dresselhaus, Phys. Rev. Lett. 95 (2005) 217403.
[31] M.S. Dresselhaus, G. Dresselhaus, R. Saito, A. Jorio, Annual reviews, in: S.R. Leone, J.T. Groves, R.F. Ismagilov, G. Richmond (Eds.), Annu. Rev. Phys. Chem. Chem. Phys. 58 (2007) 719–747
[32] M.J. O'Connell, S.M. Bachilo, X.B. Huffman, V.C. Moore, M.S. Strano, E.H. Haroz, K.L. Rialon, P.J. Boul, W.H. Noon, C. Kittrell, J. Ma, R.H. Hauge, R.B. Weisman, R.E. Smalley, Science 297 (2002) 593–596.
[33] S.M. Bachilo, M.S. Strano, C. Kittrell, R.H. Hauge, R.E. Smalley, R.B. Weisman, Science 298 (2002) 2361–2366.
[34] C. Fantini, A. Jorio, M. Souza, M.S. Strano, M.S. Dresselhaus, M.A. Pimenta, Phys. Rev. Lett. 93 (2004) 147406.
[35] Y. Zhang, H. Son, J. Zhang, M.S. Dresselhaus, J. Kong, Z. Liu, J. Phys. Chem. C 111 (2007) 1983–1987.
[36] Ge.G. Samsonidze, R. Saito, N. Kobayashi, A. Grüneis, J. Jiang, A. Jorio, S.G. Chou, G. Dresselhaus, M.S. Dresselhaus, Appl. Phys. Lett. 85 (2004) 5703–5705.
[37] V.N. Popov, N. J. Phys. 6 (2004) 17.
[38] A.G. Souza Filho, M. Endo, H. Muramatsu, T. Hayashi, Y.A. Kim, E.B. Barros, N. Akuzawa, Ge.G. Samsonidze, R. Saito, M.S. Dresselhaus, Phys. Rev. B 73 (2006) 235413.
[39] M. Endo, M. Muramatsu, T. Hayashi, Y.A. Kim, G. van Lier, J.C. Charlier, H. Terrones, M. Terrones, M.S. Dresselhaus, Nano Lett. 5 (2005) 1099–1105.
[40] M.S. Dresselhaus, G. Dresselhaus, Adv. Phys. 51 (2002) 1–186. Reprinted from M.S. Dresselhaus, G. Dresselhaus, Adv. Phys. 30 (1981).
[41] S.-H. Jhi, S.G. Louie, M.L. Cohen, Solid State Commun. 123 (2002) 495–499.
[42] E. Barros, Properties of graphitic foams and carbon nanotubes (in Portuguese), PhD thesis, Universidade Federal do Ceará, Fortaleza-CE, 60455-760, Brazil, Departamento de Física, October 2006.
[43] M.A. Pimenta, G. Dresselhaus, M.S. Dresselhaus, L.G. Cançado, A. Jorio, R. Saito, Phys. Chem. Chem. Phys. 9 (2007) 1276–1290.
[44] S.G. Chou, H. Son, J. Kong, A. Jorio, R. Saito, M. Zheng, G. Dresselhaus, M.S. Dresselhaus, Appl. Phys. Lett. 90 (2007) 131109.